Title

Surface Waveguides Supporting Both TM Mode and TE Mode With the Same Phase Velocity

Journal

IEEE Transactions on Antennas and Propagation, 64(9)

ISSN

0018-926X

Authors

Li, Mei

Xiao, Shaoqiu

Long, Jiang

et al.

Publication Date

2016-09-01

DOI

10.1109/tap.2016.2583471

Peer reviewed

Surface Waveguides Supporting Both TM Mode and TE Mode With the Same Phase Velocity

Mei Li, *Student Member IEEE*, Shaoqiu Xiao, *Member IEEE*, Jiang Long, *Student Member, IEEE*, and Daniel F. Sievenpiper, *Fellow, IEEE*

***Abstract*— Two kinds of surface-wave waveguide (SWG) topologies are proposed in this paper with the objective to achieve the property of supporting both transverse magnetic (TM) and transverse electric (TE) modes with the same phase velocity. The first type is composed of two frequency-selective surfaces (FSSs) as layers whose dominant modes are TM mode and TE mode, respectively. For illustration'C the combination of loop-type FSS and wire-grid-type FSS is analyzed and its dispersion characteristics are examined as well. The second class also consists of two layers. For the top layer, there are gaps in one direction and continuous conducting strips in the orthogonal direction. The bottom layer is created from a 90° rotation of the top layer. As a particular illustration, a modified bow-tie-like SWG structure is investigated. The simulated results show that the two proposed SWG structures exhibit the property of supporting both TM mode and TE mode with the same phase velocity over a broad bandwidth. In addition, the effects of lattice types on dispersion diagrams are discussed in this paper. Near field measurements are also carried out to validate the simulations and good agreements are achieved.**

***Index Terms*— Artificial materials, dispersion, periodic structures, surface waves (SWs), surface-wave waveguides.**

I. Introduction

SURFACE waveguides (SWG) are a class of open-boundary structures with the capability of guiding surface waves (SWs), which are intimately bound to the surface of the structure [1]. One of the most commonly studied type is the planar structures consisting of periodic subwavelength elements. Various terminologies, such as artificial impedance surfaces including scalar and tensor impedance surfaces [2]–[6], and metasurfaces [7]–[9], have been used in the literature. Here, we classify them under the broad terminology of SW waveguide (SWG) structures. Due to the capability of controlling the propagation path of SWs [10], [11], SWG have been employed for the applications of electromagnetic scattering alteration, cloaking, absorbing, and self-focusing [12]–[16]. Gradient SWG structures have been used for SW and propagating wave manipulation [17], [18]. SWG structures also have been widely employed for antenna applications in the terms of modulated reactance surfaces [19], [20], holographic surfaces [4], [21], [22], and lenses [23].

A SWG structure can support SW that are polarized in a transverse electric (TE) mode, a transverse magnetic (TM) mode, or a combination of a TM and a TE mode depending on the geometric configuration of the SWG surfaces [4]. Naturally occurring surfaces, such as a conducting plane, support a SW mode of TM type. In general, for a grounded periodic SWG structure consisting of a frequency selective surface (FSS) with electrically small cells printed on the top layer of a grounded dielectric, the dominant SW mode is also TM type no matter whether the FSS elements is a patch type or an aperture type [24]. However, for the ungrounded SWG case, the electromagnetic behavior of the SWG would change dramatically by changing very small electrical connections [25]. It is shown that a TM mode is dominantly supported when the vertexes of a geometrically self-complementary SWG are connected, and a TE mode is dominantly supported when the vertexes are disconnected. Similarly, the dominant SW is TM mode when the unit cell is a square aperture and TE mode when the unit cell is a square patch.

SWG structures that support a dominant TM mode or a TE mode have been studied for years and exploited to design holographic surfaces for applications like leaky-wave radiation and field focusing [4], [17]. However, these structures are generally sensitive to the polarization direction and therefore limitations exist due to such polarization sensitivities. For example, it is a challenge to get a centrally symmetric focused field when the modulated SWG are illuminated by a horizontally polarized field [17]. Regarding holographic antennas when excited by a horizontally polarized field, a narrow symmetric beam is hard to achieve [26]. As a result, the aperture efficiency of holographic antennas is reduced. Therefore, one significant challenge is to create a SWG structure that is insensitive to polarization. Since an incident wave can always be decomposed into TM and TE waves, supposing we have a SWG structure that can support both TM mode and TE mode with the same phase velocity, then the incident wave can

Manuscript received December 8, 2015; revised April 19, 2016; accepted June 8, 2016. Date of publication August 5, 2016; date of current version September 1, 2016. This work was supported in part by the National Science Foundation under Grant ECCS-1306055, the China Scholarship Council (CSC), in part by National High Technology Research and Development Program under Grant 2015AA7124075A, and in part by AFOSR Grant FA9550-16-1-0093.

M. Li is with the School of Physical Electronics, University of Electronic Science and Technology, Chengdu 610054, China, and also with the Department of Electrical and Computer Engineering, University of California at San Diego, La Jolla, CA 92093 USA (e-mail: limei.email@gmail.com).

S. Xiao is with the School of Physical Electronics, University of Electronic Science and Technology, Chengdu 610054, China (e-mail: xiaoshaoqiu@uestc.edu.cn).

J. Long was with the University of California, San Diego, La Jolla, CA 92093 USA. He is now with Skyworks Solution Inc., Woburn, MA 01801 USA (e-mail: longjiang.dragon@gmail.com).

D. F. Sievenpiper is with the University of California, San Diego, La Jolla, CA 92093 USA (e-mail: dsievenpiper@eng.ucsd.edu).

Color versions of one or more of the figures in this paper are available online at http://ieeexplore.ieee.org.

Digital Object Identifier 10.1109/TAP.2016.2583471

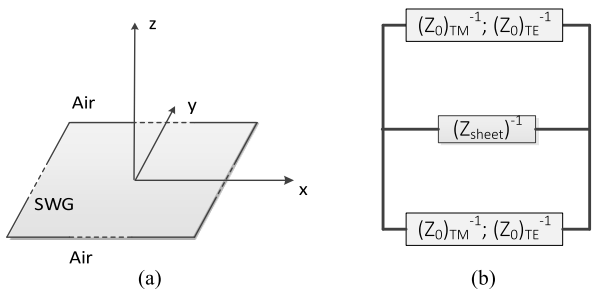

Fig. 1. Equivalent transmission line for transverse resonance analysis. (a) Infinite large SWG impedance sheet placed in the free space. (b) Transmission-line model for the SWG.

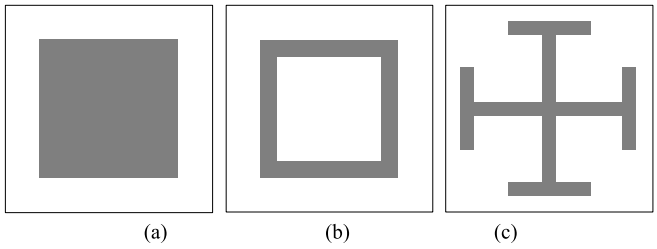

Fig. 2. FSS elements supporting TE modes. (a) Square patch. (b) Square loop. (c) Jerusalem cross.

propagate along the surface regardless of its polarization. In other words, such an SWG structure is insensitive to the polarization direction.

In this paper, we introduce two categories of SWG structures that can support both TM mode and TE mode with the same phase velocity. The proposed SWG structures are constructed by two printed layers separated by a thin dielectric substrate. The two layers of the first SWG type are formed by sub-wavelength periodic elements. The two layers can dominantly support TM mode and TE mode, respectively. For the second type of SWG structures, the bottom layer is simply a 90° rotation of the top layer with respect to the normal direction of the surface. In terms of the configuration of each layer, there are gaps in one direction and continuous conducting strips in the orthogonal direction. When examining the SW propagation characteristics of an SWG structure, the analysis results in dispersion diagrams, and another goal in this paper is to obtain TM and TE dispersion curves that are close to each other as much as possible. It is demonstrated by both simulations and measurements that the two types of SWG structures can support both TM and TE modes with the same phase velocity over a quite broad bandwidth.

This paper is organized as follows. Section II presents the theoretical analysis of a SWG structure suspended in free space using a transmission line model and the transverse resonance condition. Section III presents a SWG category constructed by two layers whose dominant modes are TM mode and TE mode, respectively. As an illustration, a loop-wire unit cell is designed and its dispersion property is investigated as well. Then in Section IV, the configuration of the second kind of SWG is depicted and a modified bow-tie-like unit cell is studied for verification. Section V investigates the effects of lattice types on dispersion curves. As last, conclusions are drawn in Section VI.

II. Theoretical Analysis of Surface Waveguide

Here, the attention is concentrated on SWG structures suspended in free space without a ground plane, as shown in Fig. 1(a). SWG structures are capable of supporting a SW mode, which is intimately bound to the surface of the structure [1]. The field is characterized by an exponential decay $e^{-k_{z0}z}$ away from the surface and having the usual propagation function $e^{-jk_x x}$ (assuming the SW mode propagates along the $+x$ direction). Here, $k_{z0}^2 = {k_x}^2 - k_0^2$, $k_{z0} > 0$ and k_0 is the wave number in the free space above the surface. The TM and TE wave impedances are therefore calculated by [27]

$$(Z_0)_{\mathrm{TM}} = \frac{E_x}{H_y} = -j\eta_0 \frac{k_{z0}}{k_0} \tag{1}$$

$$(Z_0)_{\mathrm{TE}} = -\frac{E_y}{H_x} = j\eta_0 \frac{k_0}{k_{z0}} \tag{2}$$

where η_0 is the wave impedance in the free space above the surface.

Surface impedance boundary conditions are found to be very helpful in analyzing wave propagation properties along scalar or tensor impedance surfaces [3], [4], even though not describing the details of the field distribution near the surface. Fig. 1(b) shows the transmission-line model of the SWG structure, where, Z_{sheet} represents the surface impedance of the SWG structure. According to the transverse resonance condition [28], for a TM mode, there is

$$(Z_0)_{\mathrm{TM}}^{-1} + (Z_{\mathrm{sheet}})^{-1} + (Z_0)_{\mathrm{TM}}^{-1} = 0. \tag{3}$$

Using (1) and (2) in (3) leads to

$$Z_{\mathrm{sheet}} = 2j\eta_0 \frac{k_{z0}}{k_0}. \tag{4}$$

Expression (4) manifests that in order to support a TM mode propagation along a SWG structure, the surface impedance should have inductive reactive term. By the same manner, it can be proved that in order to support a TE SW, the reactive part of the surface impedance must be capacitive. This gives a physical insight into the working mechanism of a SWG structure consisting of electrically small periodic elements, which can be analyzed by an equivalent circuit model.

III. Unit Cell Design of Loop-Wire Structure

A. Topology Configuration

The first SWG topology contains two subwavelength FSS whose dominant modes are TE and TM modes, respectively. Fig. 2 shows three of the most common FSS unit-cell geometries whose dominant modes are TE mode: square patch, square loop, and Jerusalem cross structure. The gaps between adjacent conducting patches or wires create a dominant capacitive response at low frequencies and therefore, as analyzed in Section II that a capacitive response is needed to support TE mode propagation, the dominant mode of these elements is TE mode.

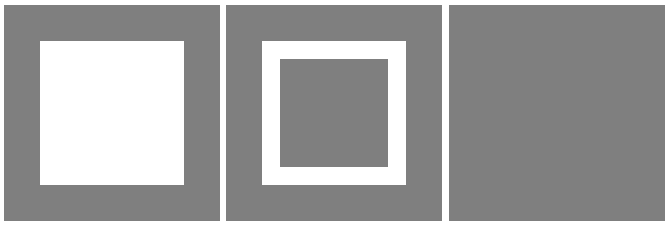

(a) (b) (c)

Fig. 3. Some typical FSS elements supporting TM modes. (a) Wire grid. (b) Ring slot. (c) Conducting ground.

Two typical FSS unit cells whose dominant modes are TM mode are shown in Fig. 3(a) and (b): wire grid and ring slot structure. They are the complementary geometries of the square patch and square loop FSS [as shown in Fig. 2(a) and (b)] whose surface impedances are capacitive. Therefore, according to the Babinet principle, their surface impedances are inductive. In fact, the inductance mainly comes from the continuous conducting strips. Especially, the dominant mode for a metal ground [as shown in Fig. 3(c)] is also TM type due to its inductive property.

It is demonstrated in the following content that a composite structure of a capacitive FSS and an inductive FSS would exhibit the property that the dispersion curves of the TM mode and the TE mode overlap at certain frequencies. In other words, the double-layer structure can support both TM mode and TE mode with the same phase velocity. Therefore, the combination of any FSS type from Fig. 2 and one Fig. 3 can achieve this property. As expected, by choosing proper dimensions, a grounded patch FSS, that is a combination of Figs. 2(a) and 3(c), can exhibit the same dispersion characteristics.

B. Unit Cell Design

The loop-wire unit cell design is illustrated in Fig. 4 (a). A square loop and a wire-grid are printed on the two sides of a 0.508-mm-thick Rogers RT/duroid 5880 substrate (εr = 2.2) with lattice dimension $p = 3.5$ mm. Fig. 4(b) illustrates a square portion of the surface containing a few unit cells. Such a loop-wire configuration has been exploited for a miniaturized-element FSS focusing on its reflection/transmission properties [29], [30]. In this paper, the emphasis is on the SWG property and thus the analysis leads to dispersion diagrams. A full-wave electromagnetic simulation software Ansys HFSS version 15.0 is utilized to examine the performance of the SWG structures.

C. Measured and Simulated Results

In simulation, only a single unit needs to be analyzed to interpret the properties of a periodic structure by assigning master-slave boundaries in the eigenmode solver. In experiment, a finite size surface consisting of 53 × 75 cells was fabricated and tested to represent the infinitely large periodic structure. A photograph of a section of the surface is shown in Fig. 5.

A near field scanner was used to do the dispersion measurement. The measurement setup for the TM mode and the TE mode are different, as is shown in Fig. 6(a) and (b), respectively. A trapezoidal microstip-line connected to one

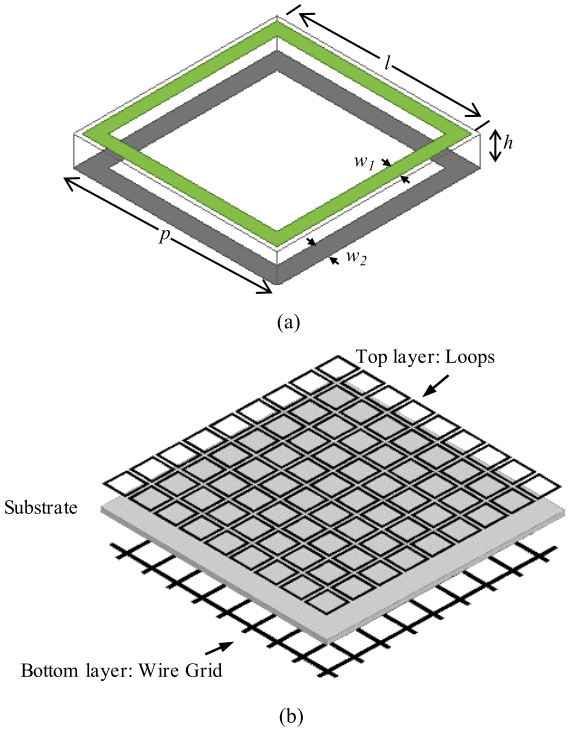

Fig. 4. Loop-wire unit cell and a small portion of its SWG. (a) Loop-wire unit cell geometry: $p = 3.5$ mm, $l = 3.4$ mm, $h = 0.508$ mm, $w_1 = 0.225$ mm, and $w_2 = 0.25$ mm. (b) SWG consisting of the loop array on one side and wire grid on the other side.

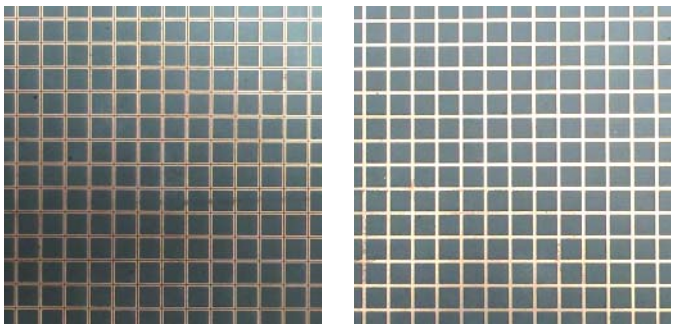

(a) (b)

Fig. 5. Photograph of a session of the finite-size surface. (a) Top side: loop FSS. (b) Bottom side: wire-grid FSS.

port of an Agilent E5071C vector network analyzer (VNA) was adopted to excite the TM mode. A vertical probe, which is scanned across the surface, was connected to the second port of the VNA so as to record the E_z field distributions. With regard to the measurement setup of TE mode, as shown in Fig. 6(b), a waveguide port was connected to one port of the VNA to excite the TE mode and a horizontal probe was connected to the second port of the VNA to record the E_y field distributions.

S_{21} of the E_z and E_y fields were recorded along a x-direction line of 150 mm with 500-um increments in the experiment. By implementing the fast Fourier transform algorithm (FFT) to the measured S_{21} along the 150-mm line, the wavenumber of the TM mode and TE mode can be extracted for the whole frequency range. Fig. 7 gives the measured and simulated dispersion diagrams of the unit-cell design with the direction of propagation along the x-direction.

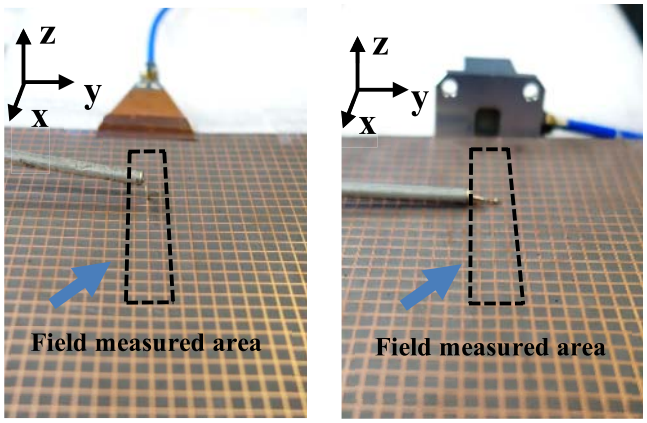

(a) (b)

Fig. 6. Near field measurement setup for (a) TM mode and (b) TE mode.

Excellent agreement is achieved between the simulation and the measurement. Due to the symmetric geometry, the same dispersion curves would be obtained when waves propagate along the y-direction. According to the simulation, the dispersion curves of the TM mode and TE mode overlap around 18 GHz, which means TM mode and TE mode have the same phase velocity.

To get a better understanding of the SW propagation property along the surface, both TM and TE field distributions of the proposed SWG structure are investigated. Fig. 8(a) and (b) shows the simulated TM mode and TE mode distributions in the xz plane, respectively. It shows obviously that the TM mode and the TE mode are tightly bound to the SWG surfaces. The TM mode and the TE mode distributions close to the xy plane are measured and shown in Fig. 8(c) and (d). As can be seen from Fig. 8(d), for the TE mode, the wavelength can be estimated from the field distributions. For the TM mode, due to the appearance of higher order modes like evanescent modes that are picked up by the vertical probe scanning above the surface at a height around 0.2 mm, the wavenumber is hard to tell from the E_z field distributions. Therefore, the FFT is utilized for both TM and TE wavenumber calibrations.

IV. Unit Cell Design of Double-Layer Modified Bow-Tie-Like Structure

A. Topology Configuration

For an array of continuous, conducting narrow strips, the impedance is either inductive (responsible for the TM mode) or capacitive (responsible for the TE mode), depending on whether the incident wave is polarized parallel to or perpendicular to the edges of the strips, respectively [1]. Fig. 9(a) shows a double-layer unit cell with 90° rotational symmetry in the xy plane. A small section of a SWG constructed by this kind of unit cell is shown in Fig. 9(b). For each layer, there are gaps in one direction and continuous strips in the orthogonal direction. Fig. 9(c) shows an example of the dispersion diagram for this kind of unit cell, which demonstrates that there is a point where the TM mode and TE mode overlap, indicating that the TM mode and TE mode have the same phase velocity. Based on this topology, two unit

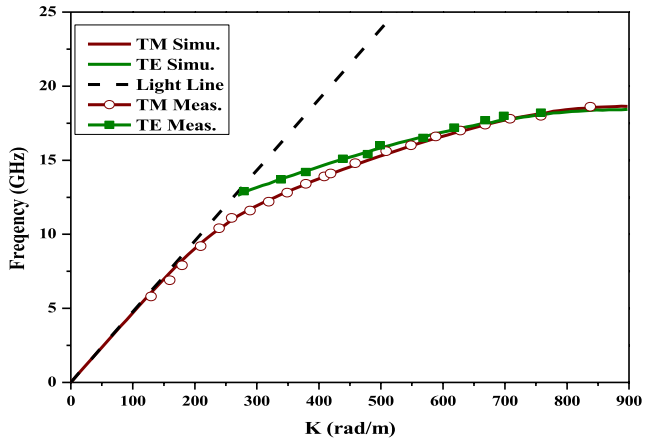

Fig. 7. Dispersion diagram of the loop-wire unit cell.

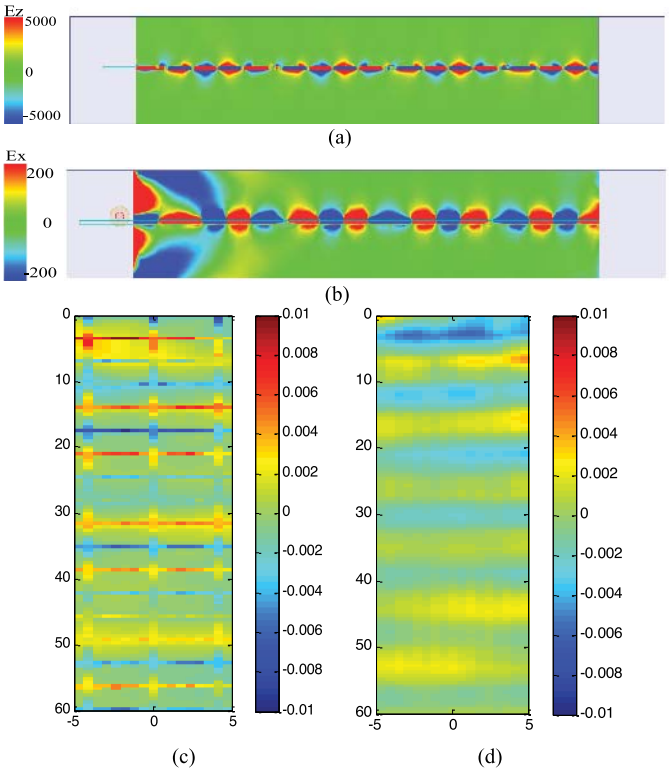

Fig. 8. Field distributions at 18 GHz of (a) simulated E_z for TM mode and (b) simulated E_y for TE mode in the xz plane, (c) measured E_z for TM mode and (d) measured E_y for TE mode close to the xy plane (at a height around 0.2 mm).

cells are proposed, as shown in Fig. 10, which give similar dispersion diagrams as that shown in Fig. 9(c). The step-like unit cell shown in Fig. 10(a) derives directly from the topology plotted in Fig. 9(a). In order to realize a miniaturization design, bow-tie-like unit in Fig. 10(b) is proposed based on Fig. 10(a). Fig. 11(b) shows the dispersion diagram for the particular bow-tie-like structure, as shown in Fig. 10(b). In order to get better performance that TM mode and TE mode give the same phase velocity during a broader bandwidth, a modified bow-tie-like structure is proposed in Section IV-B.

B. Unit Cell Design

The configuration of the bi-layer modified bow-tie-like structure and its detailed parameters are shown in Fig. 11.

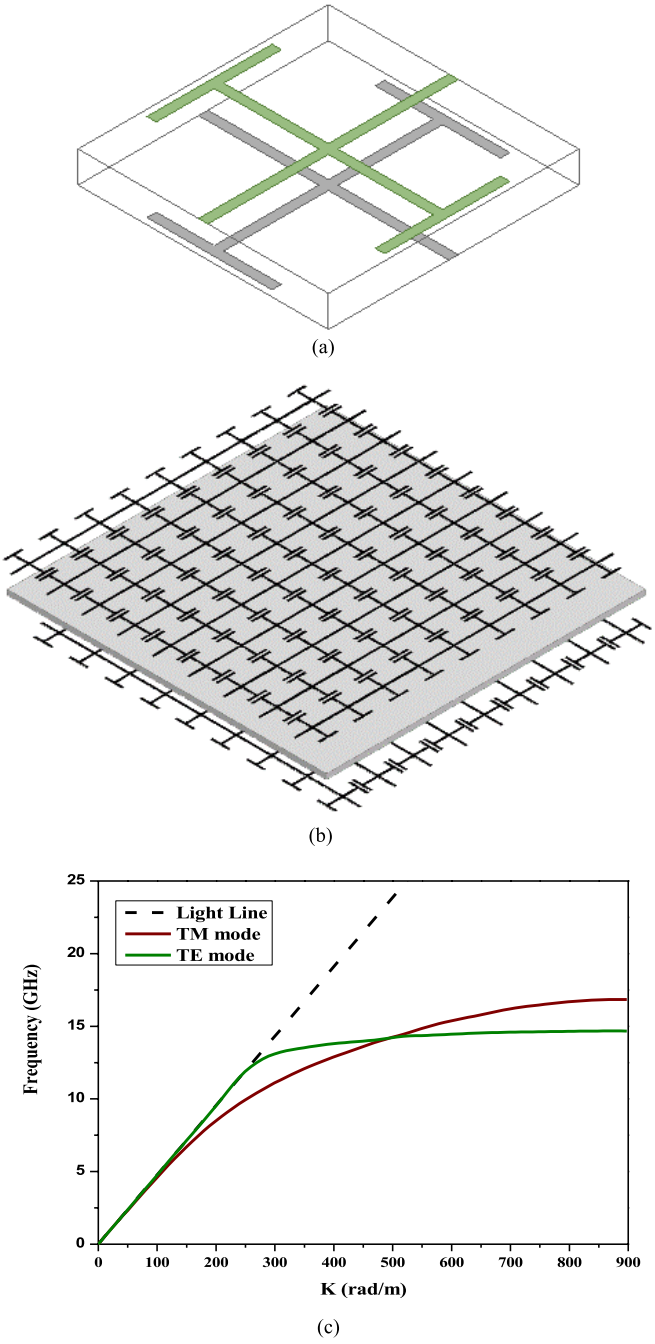

Fig. 9. Double-layer SWG and its dispersion diagram. (a) Unit cell configuration. (b) Small section of the SWG surface. (c) Example of its dispersion curves.

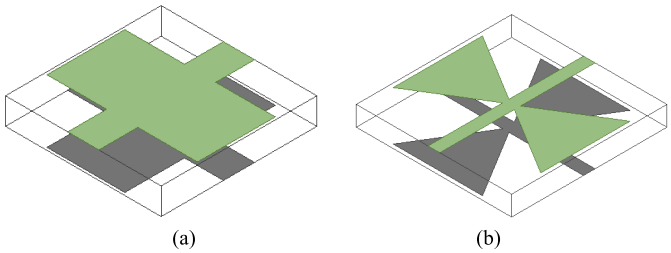

Fig. 10. Double-layer SWG unit cells. (a) Step-like unit cell. (b) Bow-tie-like unit cell.

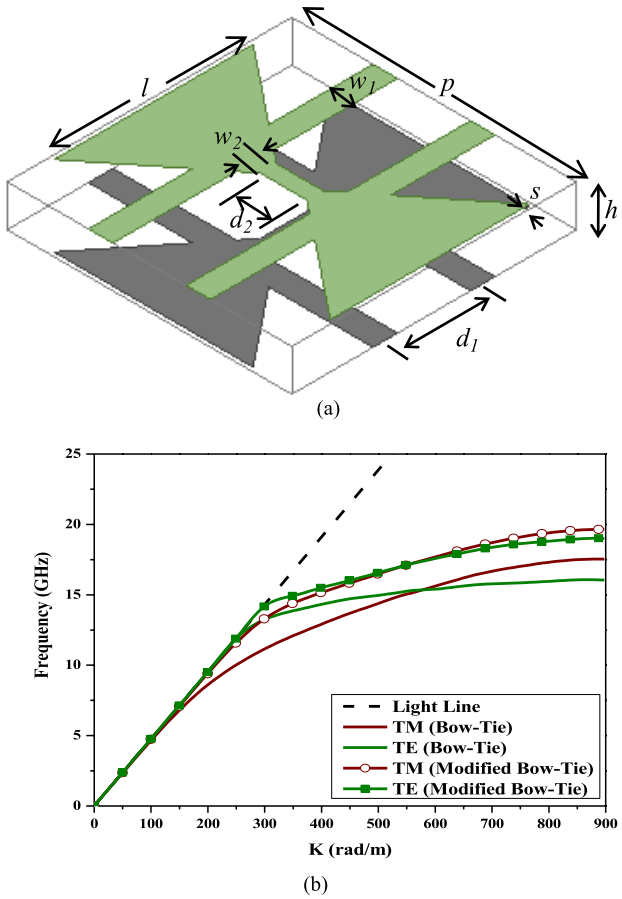

Fig. 11. Modified bow-tie-like unit cell and simulated dispersion curves. (a) Unit cell configuration: $p = 3.5$ mm, $h = 0.508$ mm, $l = 2.45$ mm, $d_1 = 1.2$ mm, $d_2 = 0.576$ mm, $s = 0.05$ mm, $w_1 = 0.3$ mm, and $w_2 = 0.2$ mm. (b) Simulated dispersion curves: the solid line corresponding to the structure in Fig. 10(b) and the line + symbol corresponding to the structure in Fig. 11(a).

Compared with the structure shown in Fig. 10(b), the central metal strip was replaced by twin wires separated with a distance of $d_1 = 1.2$ mm. Fig. 11 shows the simulated dispersion curves of the two unit cells. The dimensions of the parameters of bow-tie-like structure are kept same as that of the modified bow-tie-like structure shown in Fig. 11(a). As can be seen from Fig. 11(b), the modified bow-tie structure exhibits better performance, because the two modes have almost the same phase velocity over a broad bandwidth than that of the bow-tie-like structure.

According to the parametric study, the spacing between the twin wires, d_1, has a great effect on the cross of TM and TE modes and in what level the two modes overlap. Fig. 12 shows the dispersion diagrams with different values of d_1. As can be seen in Fig. 12, d_1 has a dramatic effect on the dispersion curve of the TE mode, whose slope increases with the increase of d_1.

C. Measured and Simulated Results

A prototype sample of the modified bow-tie-like SWG with 53×75 cells was fabricated and tested using the near field scanner. Fig. 13 shows a small section of the fabricated sample. The measurement setup for the TM mode and TE mode measurement are kept almost the same as that in Section III-C except for a horizontal probe, as shown in Fig. 14(b), was used for the TE mode excitation. The E_z and E_y fields are recorded by a vertical probe and a horizontal probe, respectively.

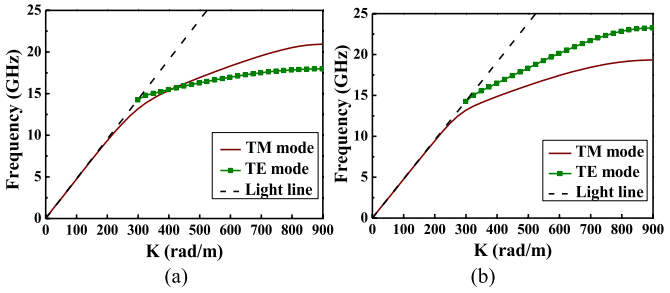

Fig. 12. Dispersion curves with different d_1. (a) $d_1 = 0.8$ mm. (b) $d_1 = 2$ mm.

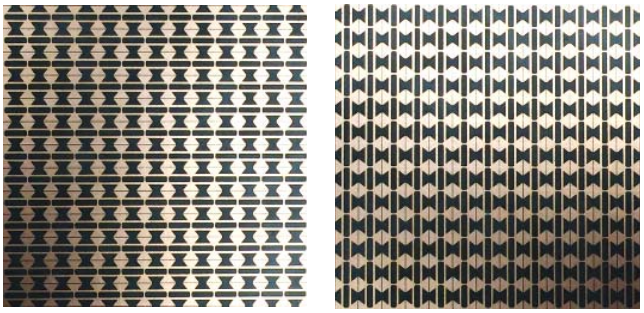

Fig. 13. Photograph of a session of the finite-size surface. (a) Top side. (b) Bottom side.

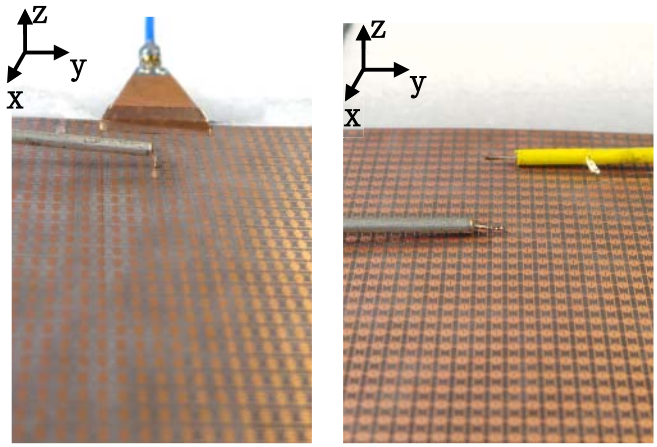

Fig. 14. Near field measurement setup for (a) TM mode measurement and (b) TE mode measurement.

The measured wavenumbers are calculated by applying the FFT algorithm to the recorded S_{21} of the E_z and E_y field distributions along a x-direction line of 150 mm at 500-um increments. Fig. 15 shows the measured dispersion curves as well as the simulated ones for comparison. The measurement and the simulation exhibits good consistency. According to the simulation, the TM mode and TE mode give the same phase velocity around 18 GHz. In addition, the dispersion curves of the two modes closely overlap. The field distributions are also simulated and measured, which demonstrates that TM and TE modes are tightly bound to the SWG surface. For the sake of brevity, the detailed TM and TE field distributions are not shown here.

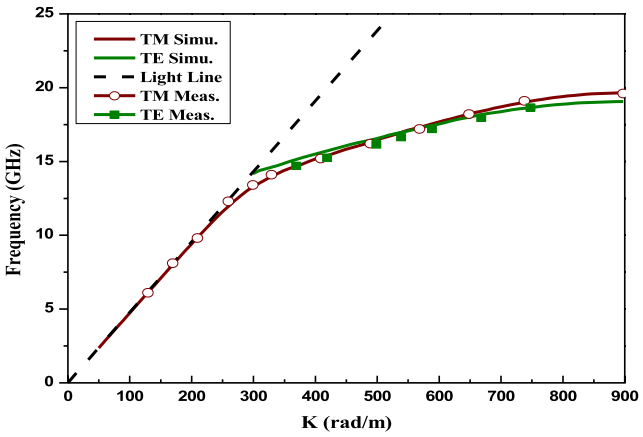

Fig. 15. Dispersion diagram of the bi-layer modified bow-tie-like unit cell.

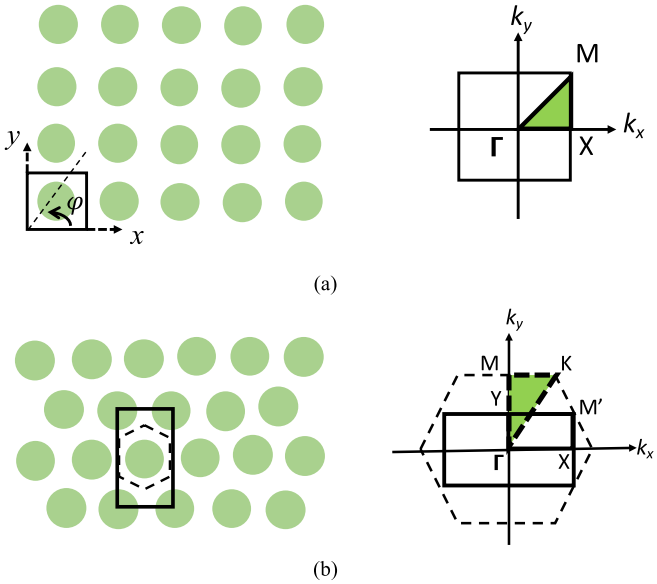

Fig. 16. Lattice types and their Brillouin zones. (a) Square lattice. (b) Hexagonal lattice.

V. Effects of Lattice Types on Dispersion Curves

A 2-D square and hexagonal lattices are two commonly seen lattice types, which have been widely studied in the field of photonic crystals and electromagnetic bandgap structures. It has been reported that the geometry of photonic crystal lattice types would significantly affect the bandgap characteristics [31], [32], and laser characteristics, such as threshold conditions and lasing spectra [33]. The lattice structures and Brillouin zones for these two types are shown in Fig. 16, where the green shadow triangles indicate the irreducible Brillouin zones. For the sake of calculation, as shown in Fig. 16(b), a rectangular unit supercell (solid rectangular) instead of a hexagonal one (dashed hexagon) is chosen for simulation and therefore the corresponding first Brillouin zone is the solid rectangular instead of the hexagonal lattice [34]. The irreducible Brillouin zone of the rectangular lattice is indicated by path ΓXM′YΓ. Note that, due to the folding of both reciprocal lattices, scanning along the contour ΓXM′YΓ completely covers the whole Brillouin zone of the hexagonal lattice.

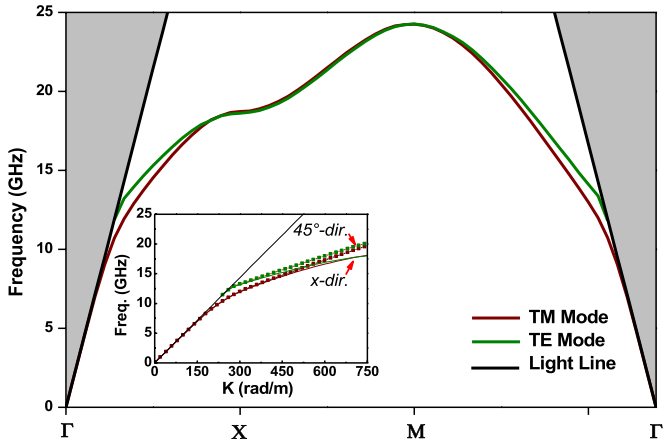

Fig. 17. Dispersion diagram of the first two modes of the loop-wire SWG with square lattice. The subgraph indicates the dispersion curves along the x-direction and the 45° direction.

This paper aims to investigate propagation characteristics of SWGs. Ideally, the proposed SWG surfaces can support both TM- and TE-mode with the same phase velocity in an arbitrary direction along the surface. Due to the symmetric configuration in the xy plane, here, the loop-wire SWG topology is analyzed to study the effects of lattice types on dispersion curves. Two lattice structures, square, and hexagonal lattices, are examined in this paper. The SWG configuration proposed in Section III is a square lattice. Fig. 17 shows the simulated dispersion diagrams of the loop-wire SWG with square lattice in the cases of the first two modes, where the subgraph shows when the two modes propagate in the x-axis [path Γ-X in Fig. 16(a)] and the diagonal [path Γ-M in Fig. 16(a)] directions. The SWG geometry and parameters are kept the same with those presented in Section III. As can be seen from Fig. 17, the dispersion curves in the two directions are aligned with each other in the low frequency range. However, with the increase of frequency, the discrepancy deteriorates. As a result, the dispersion curves of the loop-wire SWG with square lattice exhibit great discrepancy when the SWs propagate in different directions along the SWG surface.

Now, let us examine the loop-wire SWG topology with hexagonal lattice. As shown in Fig. 18(a), a rectangular supercell consisted by hexagonal unit cells in terms of discrete loop-FSS for the top layer and continuous wire-FSS for the bottom layer is presented. A small portion of the corresponding SWG with hexagonal lattice is shown in Fig. 18(b). The dispersion diagram of the first two modes of the supercell is given in Fig. 19. The subgraph illustrates the simulated dispersion curves when the two modes propagate along the y-axis [path Γ-M in Fig. 16(b)] and $\varphi = 60°$ [path Γ-K Fig. 16(b)] directions. According to Fig. 19, the proposed hexagonal loop-wire SWG with hexagonal lattice exhibits almost the same dispersion curves when SWs propagate in different directions of the surface. Therefore, SWGs with hexagonal lattice exhibit better performance in the aspect of dispersion property than those with square lattice.

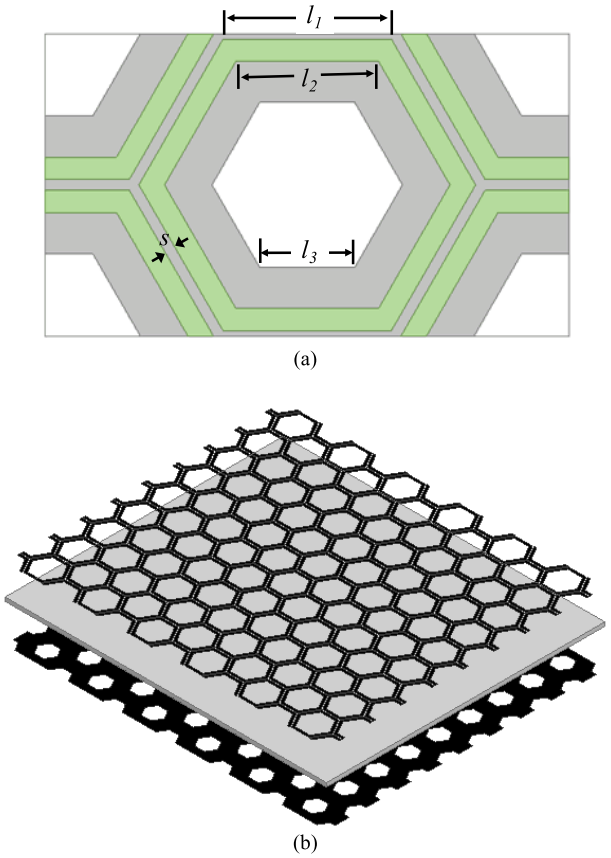

Fig. 18. Hexagonal loop-wire unit supercell and its SWG configuration with hexagonal lattice. (a) Hexagonal loop-wire unit: $l_1 = 2.3$ mm, $l_2 = 1.95$ mm, $l_3 = 1.3$ mm, and $s = 0.075$ mm. (b) Portion of SWG with hexagonal lattice. The thickness of the substrate is 0.508 mm.

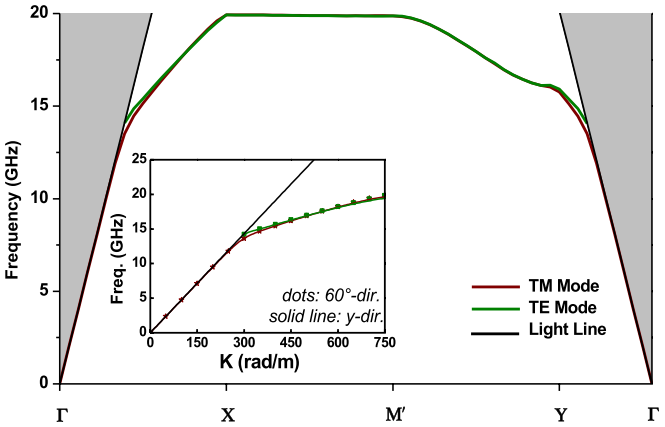

Fig. 19. Dispersion diagram of the first two modes of the loop-wire SWG with hexagonal lattice. The subgraph indicates the dispersion curves along the y-direction and the 60° direction.

Fabrication and measurements have been carried out and the measurement setup is the same as that shown in Fig. 14. The simulated and measured dispersion curves for the TM mode and TE mode that propagate along the y-axis and $\varphi = 60°$ directions are given in Fig. 20(a)–(d), respectively. The same FFT method that described in

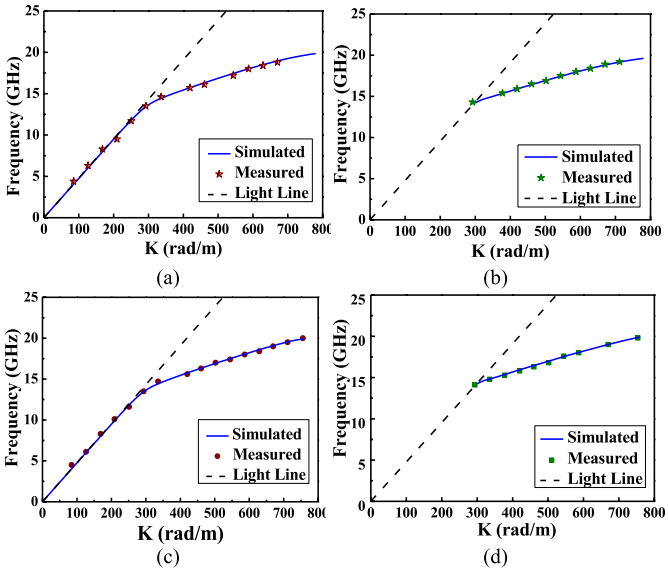

Fig. 20. Measured and simulated dispersion curves of (a) TM mode propagating along the y-axis direction, (b) TE mode propagating along the y-axis direction, (c) TM mode propagating along the $\varphi = 60°$ direction, and (d) TE mode propagating along the $\varphi = 60°$ direction.

Sections III and IV is utilized to obtain the measured dispersion curves. As shown in Fig. 20, the simulation and the measurement agree well with each other.

VI. Conclusion

Two SWG topologies are found to have the property of supporting both TM mode and TE mode with the same phase velocity. The first type consists of two FSS layers whose dominant modes are TM mode and TE mode, respectively. The second type is composed of two layers and the bottom layer comes from a 90° rotation from the top layer. The top layer has gaps in the x-direction and continuous conducting strips in the y-direction. Therefore, in either the x-direction or y-direction, there are gaps on one layer and continuous conducting strips on the other layer. Based on these topologies, SWG structures with various unit-cell shapes can be created to obtain the desired characteristics. Since various FSS shapes can be found to support TM mode or TE mode, according to the first type of the proposed SWG topologies, the combination of any FSS whose dominant mode is TM mode and any one whose dominant mode is TE mode can achieve these characteristics. For the second type, several unit cells are proposed in this paper, and many other shapes can also be created based on this topology. SWG surfaces with these characteristics of supporting both TM and TE mode with the same phase velocity have great potential to be used in many applications like gradient Luneberg lens antennas and holographic surfaces. For instance, a planar holographic surface with central focusing property can be achieved when imposed by a horizontal polarized excitation.

References

[1] R. E. Collin, *Field Theory of Guided Waves*. New York, NY, USA: McGraw-Hill, 1960.

[2] H. J. Bilow, "Guided waves on a planar tensor impedance surface," *IEEE Trans. Antennas Propag.*, vol. 51, no. 10, pp. 2788–2792, Oct. 2003.

[3] B. H. Fong, J. S. Colburn, J. J. Ottusch, J. L. Visher, and D. F. Sievenpiper, "Scalar and tensor holographic artificial impedance surfaces," *IEEE Trans. Antennas Propag.*, vol. 58, no. 10, pp. 3212–3221, Oct. 2010.

[4] A. M. Patel and A. Grbic, "Effective surface impedance of a printed-circuit tensor impedance surface (PCTIS)," *IEEE Trans. Microw. Theory Techn.*, vol. 61, no. 4, pp. 1403–1413, Apr. 2013.

[5] R. G. Quarfoth and D. F. Sievenpiper, "Nonscattering waveguides based on tensor impedance surfaces," *IEEE Trans. Antennas Propag.*, vol. 63, no. 4, pp. 1746–1755, Apr. 2015.

[6] R. Quarfoth and D. Sievenpiper, "Artificial tensor impedance surface waveguides," *IEEE Trans. Antennas Propag.*, vol. 61, no. 7, pp. 3597–3606, Jul. 2013.

[7] S. Maci, G. Minatti, M. Casaletti, and M. Bosiljevac, "Metasurfing: Addressing waves on impenetrable metasurfaces," *IEEE Antennas Wireless Propag. Lett.*, vol. 10, pp. 1499–1502, 2011.

[8] X. Li, S. Xiao, B. Cai, Q. He, T. J. Cui, and L. Zhou, "Flat metasurfaces to focus electromagnetic waves in reflection geometry," *Opt. Lett.*, vol. 37, no. 23, pp. 4940–4942, Dec. 2012.

[9] M. Mencagli, E. Martini, and S. Maci, "Surface wave dispersion for anisotropic metasurfaces constituted by elliptical patches," *IEEE Trans. Antennas Propag.*, vol. 63, no. 7, pp. 2992–3003, Jul. 2015.

[10] D. J. Gregoire and A. V. Kabakian, "Surface-wave waveguides," *IEEE Antennas Wireless Propag. Lett.*, vol. 10, pp. 1512–1515, 2011.

[11] F. Elek, B. B. Tierney, and A. Grbic, "Synthesis of tensor impedance surfaces to control phase and power flow of guided waves," *IEEE Trans. Antennas Propag.*, vol. 63, no. 9, pp. 3956–3962, Sep. 2015.

[12] R. Quarfoth and D. Sievenpiper, "Surface wave scattering reduction using beam shifters," *IEEE Antennas Wireless Propag. Lett.*, vol. 13, pp. 963–966, 2014.

[13] R. Quarfoth and D. Sievenpiper, "Alteration of electromagnetic scattering using hard and soft anisotropic impedance surfaces," *IEEE Trans. Antennas Propag.*, vol. 63, no. 10, pp. 4593–4599, Oct. 2015.

[14] P.-Y. Chen and A. Alù, "Mantle cloaking using thin patterned metasurfaces," *Phys. Rev. B*, vol. 84, p. 205110, Nov. 2011.

[15] H. Wakatsuchi, S. Kim, J. J. Rushton, and D. F. Sievenpiper, "Waveform-dependent absorbing metasurfaces," *Phys. Rev. Lett.*, vol. 111, no. 24, p. 245501, 2013.

[16] Z. Lou, X. Chen, J. Long, R. Quarfoth, and D. Sievenpiper, "Self-focusing of electromagnetic surface waves on a nonlinear impedance surface," *Appl. Phys. Lett.*, vol. 106, no. 21, p. 211102, 2015, doi: 10.1063/1.4921913.

[17] X. Wan, Y. B. Li, B. G. Cai, and T. J. Cui, "Simultaneous controls of surface waves and propagating waves by metasurfaces," *Appl. Phys. Lett.*, vol. 105, no. 12, p. 121603, 2014, doi: 10.1063/1.4896540.

[18] S. Sun, Q. He, S. Xiao, Q. Xu, X. Li, and L. Zhou, "Gradient-index meta-surfaces as a bridge linking propagating waves and surface waves," *Nature Mater.*, vol. 11, no. 5, pp. 426–431, May 2012.

[19] A. A. Oliner and A. Hessel, "Guided waves on sinusoidally–modulated reactance surfaces," *IRE Trans. Antennas Propag.*, vol. 7, no. 5, pp. S201–S208, Dec. 1959.

[20] A. M. Patel and A. Grbic, "A printed leaky-wave antenna based on a sinusoidally-modulated reactance surface," *IEEE Trans. Antennas Propag.*, vol. 59, no. 6, pp. 2087–2096, Jun. 2011.

[21] S. Pandi, C. A. Balanis, and C. R. Birtcher, "Design of scalar impedance holographic metasurfaces for antenna beam formation with desired polarization," *IEEE Trans. Antennas Propag.*, vol. 63, no. 7, pp. 3016–3024, Jul. 2015.

[22] G. Minatti, F. Caminita, M. Casaletti, and S. Maci, "Spiral leaky-wave antennas based on modulated surface impedance," *IEEE Trans. Antennas Propag.*, vol. 59, no. 12, pp. 4436–4444, Dec. 2011.

[23] M. Bosiljevac, M. Casaletti, F. Caminita, Z. Sipus, and S. Maci, "Non-uniform metasurface Luneburg lens antenna design," *IEEE Trans. Antennas Propag.*, vol. 60, no. 9, pp. 4065–4073, Sep. 2012.

[24] O. Luukkonen *et al.*, "Simple and accurate analytical model of planar grids and high-impedance surfaces comprising metal strips or patches," *IEEE Trans. Antennas Propag.*, vol. 56, no. 6, pp. 1624–1632, Jun. 2008.

[25] D. González-Ovejero, E. Martini, and S. Maci, "Surface waves supported by metasurfaces with self-complementary geometries," *IEEE Trans. Antennas Propag.*, vol. 63, no. 1, pp. 250–260, Jan. 2015.

[26] C. Rusch, J. Schäfer, H. Gulan, P. Pahl, and T. Zwich, "Holographic mmW-antennas with TE_0 and TM_0 surface wave launchers for frequency-scanning FMCW-radars," *IEEE Trans. Antennas Propag.*, vol. 63, no. 4, pp. 1603–1613, Apr. 2015.

[27] R. F. Harrington, *Time-Harmonic Electromagnetic Fields*. New York, NY, USA: McGraw-Hill, 1961, pp. 129–132.

[28] R. Sorrentino, "Transverse resonance technique," in *Numerical Techniques for Microwave and Millimeter-Wave Passive Structures*, T. Itoh, Ed. New York, NY, USA: Wiley, 1989, pp. 133–213.
[29] F. Bayatpur and K. Sarabandi, "Single-layer high-order miniaturized-element frequency-selective surfaces," *IEEE Trans. Microw. Theory Techn.*, vol. 56, no. 4, pp. 774–781, Apr. 2008.
[30] K. Sarabandi and N. Behdad, "A frequency selective surface with miniaturized elements," *IEEE Trans. Antennas Propag.*, vol. 55, no. 5, pp. 1239–1245, May 2007.
[31] J. Zha, Z. Y. Zhong, H. W. Zhang, Q. Y. Wen, and Y. X. Li, "Differences of band gap characteristics of square and triangular lattice photonic crystals in terahertz range," *J. Electron. Sci. Technol. China*, vol. 7, no. 3, pp. 268–271, 2009.
[32] P. R. Villeneuve and M. Piche, "Photonic band gaps in two-dimensional square and hexagonal lattices," *Phys. Rev. B*, vol. 46, no. 8, pp. 4969–4972, 1992.
[33] T.-T. Wu, C.-C. Chen, and T.-C. Lu, "Effects of lattice types on GaN-based photonic crystal surface-emitting lasers," *IEEE J. Sel. Topics Quantum Electron.*, vol. 21, no. 1, Jan./Feb. 2015, Art. no. 1700106.
[34] R. Antos and M. Veis, "Fourier factorization with complex polarization bases in the plane-wave expansion method applied to two-dimensional photonic crystals," *Opt. Exp.*, vol. 18, no. 26, pp. 27522–27524, 2010.

Mei Li (S'15) received the B.S. degree in electronic information science and technology from the Chengdu University of Information Technology, Chengdu, China, in 2010, and the Ph.D. degree in radio physics from the University of Electronic Science and Technology of China, Chengdu, in 2016.

She was a Visiting Graduate Student with the Applied Electromagnetics Research Group, University of California at San Diego, La Jolla, CA, USA, from 2014 to 2016. Her current research interests include reconfigurable antennas, phased arrays, artificial electromagnetic structures, and holographic metasurfaces.

Shaoqiu Xiao (M'05) received the Ph.D. degree in electromagnetic field and microwave engineering from the University of Electronic Science and Technology of China (UESTC), Chengdu, China, in 2003.

He joined UESTC as an Assistant Professor in 2004. From 2004 to 2006, he was with the Wireless Communications Laboratory, National Institute of Information and Communications Technology of Japan, Koganei, Japan, as a Researcher with the focus on the planar antenna and smart antenna design and optimization. From 2006 to 2010, he was an Associate Professor with UESTC, where he is currently a Professor. He has authored/co-authored more than 160 technical journals, conference papers, books, and book chapters. His current research interests include planar antenna and phased array, microwave passive circuits, and time reversal electromagnetics.

Jiang Long (S'11) received the B.S. and M.S. degrees from Zhejiang University, Hangzhou, China, in 2007 and 2010, respectively, and the Ph.D. degree from the University of California at San Diego, La Jolla, CA, USA, in 2015.

He is currently an RF Engineer with Skyworks Solution Inc., Woburn, MA, USA. His current research interests include non-Foster circuits in antenna/microwave applications, including non-Foster circuit loaded active fast-wave waveguides, broadband metasurfaces, broadband antennas, and active microwave components.

Dr. Long received the IEEE MTT-S Graduate Fellowship in 2015.

Daniel F. Sievenpiper (M'94–SM'04–F'09) received the B.S. and Ph.D. degrees in electrical engineering from the University of California at Los Angeles, Los Angeles, CA, USA, in 1994 and 1999, respectively.

He was the Director of the Applied Electromagnetics Laboratory with HRL Laboratories, Malibu, CA, USA, prior to 2010, where his research included in artificial impedance surfaces, conformal antennas, tunable and wearable antennas, and beam steering methods. He is currently a Professor with the University of California at San Diego, La Jolla, CA, USA, where his research focuses on antennas and electromagnetic structures. He holds more than 70 issued patents and over 80 technical publications.

Dr. Sievenpiper received the URSI Issac Koga Gold Medal in 2008. Since 2010, he has served as an Associate Editor of the IEEE *Antennas and Wireless Propagation Letters*.